2011

Characterization of oxidation resistant Fe@M (M=Cr, Ni) core@shell nanoparticles prepared by a modified reverse micelle reaction

Sweta H. Naik
Virginia Commonwealth University

Kyler J. Carroll
Virginia Commonwealth University

Everett E. Carpenter
Virginia Commonwealth University, ecarpenter2@vcu.edu

Characterization of oxidation resistant Fe@M (M=Cr, Ni) core@shell nanoparticles prepared by a modified reverse micelle reaction

Sweta H. Naik, Kyler J. Carroll, and Everett E. Carpenter[a)]
Department of Chemistry, Virginia Commonwealth University, Richmond, Virginia 23284, USA

Iron-based nanoparticles are the forerunners in the field of nanotechnology due to their high magnetization saturation and biocompability which affords them use in a variety of applications. However, iron-based nanoparticles, due to a high surface-to-volume ratio, suffer from oxidation and limit its practicality by lowering the magnetic moment significantly. To avoid this oxidation, the surfaces of the particles have to be passivated. One such way to accomplish this passivation is to synthesize core@shell nanoparticles that have a surface treatment of chromium or nickel. These core@shell nanoparticles have been synthesized using a reverse micelle technique. The Cr and Ni passivated iron nanoparticles were characterized by x-ray diffraction, transmission electron microscopy, vibrating sample magnetometry, and x-ray photoelectron spectroscopy to determine their phase, morphology, surface properties, and magnetization saturation. A high magnetization saturation of 160 and 165 emu/g for Cr and Ni passivated iron core@shell nanoparticles was achieved. © *2011 American Institute of Physics*. [doi:10.1063/1.3548828]

I. INTRODUCTION

Iron-based nanoparticles are desirable for many practical applications like magnetic fluids, catalysis, magnetic storage media, and for novel biomedical applications like targeted drug delivery and biosensors due to their unique properties.[1–3] Iron has the highest magnetic moment per gram of an elemental material (up to 220 emu/g). However, the utility of the iron nanoparticles has been limited due to their ease of oxidation, which leads to the reduction in the original magnetic moment of the material. One of the most sought approaches for controlling the oxidation is to synthesize core@shell nanoparticles having a metallic core and a passivating shell. Various synthetic techniques like thermolysis, chemical precipitation, sol-gel processes, vapor deposition, and reverse micelle techniques have been utilized to synthesize these core@shell nanoparticles.[4–8]

This work describes the characterization of the iron core@shell nanoparticles passivated by chromium and nickel using a reverse micelle technique, which has been very well established in literature.[5,9] The reverse micelle technique is ideal for the synthesis of core@shell nanoparticles as it allows for the control of the surface oxidation of the particles, the size, and size distributions.[5] Chromium and nickel display superior corrosion resistant properties that make them an ideal passivating agent.[10,11] The focus of this work is to investigate the role of chromium and nickel as protective shells for the synthesis of air stable iron-based nanoparticles with enhanced magnetization saturation.

II. EXPERIMENT

Oxidation resistant Fe@M (M=Cr, Ni) core@shell nanoparticles were synthesized using a reverse micelle method similar to those found in the literature.[9,12] Cetyltrimethylammonium bromide (CTAB) was used as the surfactant, chloroform as the oil phase and aqueous reactants as the water phase. Briefly, to the 0.5 M CTAB solution in chloroform, aqueous iron (II) chloride tetrahydrate (FeCl$_2$.4H$_2$O) was added to form a transparent green reverse micelle solution. Sodium borohydride (NaBH$_4$) was then added to the micelle solution to reduce the metal precursor, turning black instantaneously due to the formation of metallic iron. The reaction was then allowed to stir for 15 min for the complete reduction of the precursor to a metallic state. An additional micelle solution was added to the reaction mixture containing aqueous chromium (III) chloride hexahydrate (CrCl$_3$.6H$_2$O) or nickel (II) chloride hexahydrate (NiCl$_2$.6H$_2$O) to form a passivating shell. The Cr or Ni precursors were reduced by the excess of sodium borohydride present in the system. The reaction mixture is allowed to age for 5 min before being quenched with 100 ml of methanol. The passivated magnetic nanoparticles are removed from the reaction mixture by magnetic separation using a rare-earth permanent magnet and washed several times with methanol to remove adsorbed surfactant from the particle surface.

The nanoparticles were characterized by transmission electron microscopy (TEM), x-ray diffraction (XRD), vibrating sample magnetometer (VSM), and x-ray photoelectron spectroscopy (XPS) to determine morphology, composition, magnetic properties, and surface characteristics. Powder XRD measurements were performed using a Panalytical X'pert pro diffractometer at a scanning step of 0.05° with a 2θ range from 15° to 80° using a graphite monochromated Cu Kα radiation source. Samples were ground and pressed onto a no-background, low-volume holder. Room temperature magnetometry was performed on a Lakeshore Cryotonics model 7300 VSM with an applied field between −10/000 and 10/000 Oe. TEM was performed with Carl Zeiss

---

a)Author to whom correspondence should be addressed. Electronic mail: ecarpenter2@vcu.edu.

109, 07B519-1

LIBRA®120 PLUS electron microscope equipped with a Gatan digital camera to determine the size and morphology of the synthesized passivated iron core@shell nanoparticles. XPS was performed on a Thermo Scientific ESCALAB 250 microprobe with a focused monochromatic Al $K\alpha$ x-ray (1486.6 eV) source and a 180° hemispherical analyzer with a six-element multichannel detector. Charge compensation was employed during data collection by using an internal flood gun (2 eV electrons) and a low-energy Ar^+ external flood gun. Binding energies of the photoelectron are corrected to the aliphatic hydrocarbon C 1s peak at 284.6 eV.

III. RESULTS AND DISCUSSION

The powder XRD pattern of the as-synthesized iron core@shell nanoparticles passivated by chromium and nickel shows a body centered cubic iron phase with no crystalline Cr, Ni, or iron oxide impurities. Figure 1 shows XRD patterns of the as-synthesized Fe@M (M=Cr, Ni) nanoparticles with an overlay of the data obtained from the JSPDS reference powder diffraction patterns of α-iron, chromium, and nickel.[9] Previous work suggests that the passivation of the iron nanoparticles was achieved with a negligible amount of Cr or Ni being incorporated into the nanoparticles.[4,5]

The magnetic properties of the passivated iron nanoparticles were measured at room temperature using a VSM. Figure 2 shows hysteresis plots of the Fe@M nanoparticles. The saturation magnetization was found to be about 130 and 135 emu/g, respectively, for Cr and Ni passivated particles. Thermogravimetric analysis was performed on a TA instruments Q5000 thermogravimetric analyzer, which showed approximately 14% weight loss. After mass correction the saturation magnetization of the Fe@M nanoparticles was found to be 160 and 165 emu/g for Cr and Ni, respectively. The passivation of the iron core is evident in the stability of the saturation magnetization. After 3 mo there is only a 10% reduction in the saturation magnetization, which is in agreement with the literature values.[5] Although it is uncertain as to what is contributing to the excess coercivity seen in the Fe@Cr sample, it is likely that it is due to a layer of antiferromagnetic Cr-oxide on the surface of the nanoparticles,

FIG. 2. (Color online) Room temperature VSM data plotted as magnetization (electromagnetic unit per gram) vs applied field (Oersted) for the Fe@M (M=Cr,Ni) core@shell nanoparticles.

whereas the Fe@Ni has a lower coercivity due to the formation of ferromagnetic metallic Ni shell. This could also explain the slight exchange bias present in the Fe@Cr sample, although the exact explanation is not clear. The structure of the shell is further alluded to XPS analysis.

Figure 3 presents TEM images of the as-synthesized Fe@M (M=Cr, Ni) core@shell nanoparticles. Both chromium and nickel passivated iron nanoparticles are relatively uniform in size with an average diameter of 7 and 10 nm, respectively. All of this characterization helped confirm that the synthesis of the core@shell nanoparticles was replicated from literature references. The role of the nickel and chromium in the passivation of the nanoparticles and thus partially explaining their oxidation stability was determined using XPS.

Figures 4(a) and 4(b) present the XPS survey scans of both the Fe@Ni and Fe@Cr nanoparticles, respectively. The photoelectron peaks reveal that the surface chemistry consists of O, C, Fe, and Cr and Ni. Detailed depth profile region scans for Fe 2p is also shown in Fig. 4(c), along with the depth profile analysis of the Ni 2p region [Fig. 4(d)]. From Figs. 4(c) and 4(d) it is evident that etch level one, corresponding to the surface of the nanoparticles, is predominantly in the form of metallic Ni 2p, whereas the Fe 2p region scans show a relatively low intensity of Fe. During
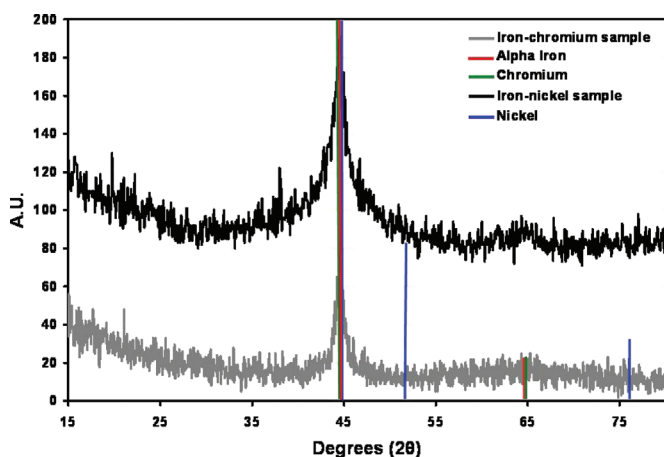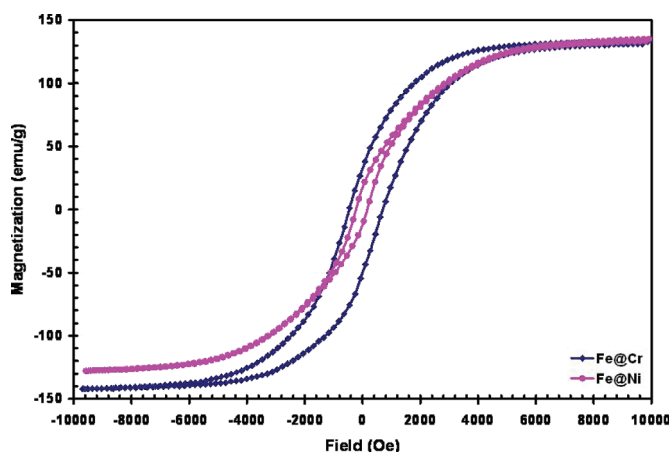

FIG. 1. (Color online) XRD pattern of the as-synthesized Fe@M nanoparticles with an overlay of the data obtained from the JSPDS reference powder diffraction patterns of α-iron, chromium, and nickel
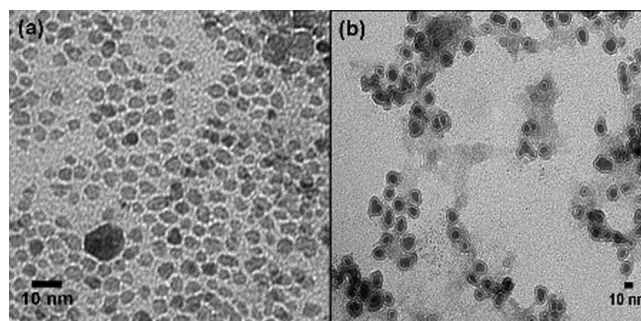

FIG. 3. TEM image of (a) Fe@Cr and (b) Fe@Ni core@shell nanoparticles synthesized by the reverse micelle technique. Both Fe@Cr and Fe@Ni nanoparticles are relatively uniform sized with an average diameter of 7 and 10 nm, respectively.
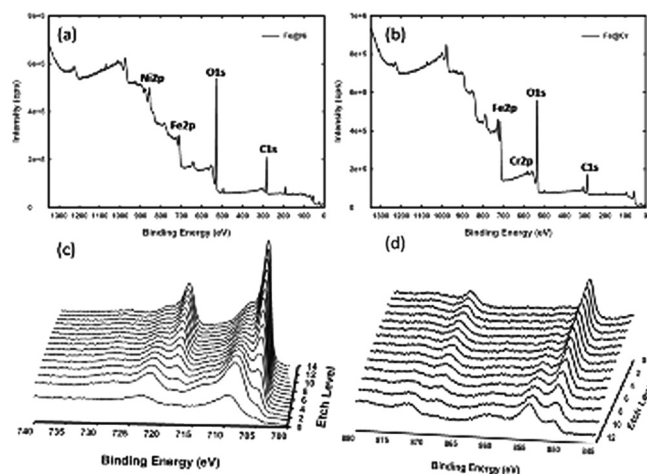
FIG. 4. XPS survey scans of (a) Fe@Ni nanoparticles and (b) Fe@Cr nanoparticles. (c) Depth profile of Fe 2*p* region scans and (d) depth profile of Ni 2*p* regions scans of Fe@Ni core@shell nanoparticles.

XPS etching, you can see that the Ni surface decreases, whereas the Fe increases, suggesting core@shell morphology. Table I lists the atomic percentages corresponding to different XPS etch levels. From Table I you can see that a majority of the surface consists of carbon and oxygen, which can be described by adsorbed organic reactants from the synthesis. This is supported by the TGA data presented earlier. However, it is evident that at etch level 0 (no etching) the samples contain a larger atomic percentage of the passivation material (Cr and Ni) and after 13 etch levels the atomic percentage decreases below 5%. In addition, the Fe 2*p*3 region

TABLE I. The atomic percentage of each element present during various XPS depth profiling etch levels.

	Etch level 0		Etch level 13
Element	Atomic percentage (%)	Element	Atomic percentage (%)
XPS depth profile of Fe@NI core@shell nanoparticles			
Fe 2*p*3	5.03	Fe 2*p*3	28.84
Ni 2*p*3	28.41	Ni2*p*3	3.27
O 1*s*	25.03	O1s	34.93
C 1*s*	41.53	C1s	32.96
XPS depth profile of Fe@Cr core@shell nanoparticles			
Fe 2*p*3	8.12	Fe2*p*3	31.85
Cr 2*p*3	16.34	Cr2*p*3	1.42
O 1*s*	32.09	O1s	33.56
C 1*s*	43.45	C1s	33.17

increases from below 10% at no etching to above 25% after 13 etch levels. It is easily distinguishable in the XPS scans that the Cr is present in an oxidized state, whereas the Ni is in its elemental form. However, the exact structure of the Cr oxide is not clear from the current XPS study.

IV. CONCLUSION

In conclusion, oxidation resistant iron core@shell nanoparticles passivated by chromium and nickel were synthesized by a reverse micelle technique producing uniformly sized particles. The use of Cr and Ni as a passivation layer on Fe nanoparticles results in particles with magnetic saturation values of 160 and 165 emu/g, respectively. The particles are found to be air stable with a minimal loss in the magnetic moment after three months. The Ni was found to reduce on the surface, giving a shell containing metallic Ni, whereas the Cr is predominately in the form of Cr-oxide. This helps reduce the coercivity in the Fe@Ni samples compared to those of the Fe@Cr samples with both of the samples showing a similar saturation magnetization.

[1]S. Naik and E. E. Carpenter, J. Appl. Phys. **103**, 07A313 (2008).
[2]G. F. Goya, V. Grazu, and M. R. Ibarra, Curr. Nanosci. **4**, 1 (2008).
[3]K. J. Carroll, M. D. Shultz, P. P. Fatouros, and E. E. Carpenter, J. Appl. Phys. **107**, 09B304 (2010).
[4]M. A. Willard, L. K. Kurihara, E. E. Carpenter, S. Calvin, and V. G. Harris, Int. Mater. Rev. **49**, 125 (2004).
[5]E. E. Carpenter, S. Calvin, R. M. Stroud, and V. G. Harris, Chem Mater **15**, 3245 (2003).
[6]C. Burda, X. B. Chen, R. Narayanan, and M. A. El-Sayed, Chem. Rev. **105**, 1025 (2005).
[7]F. Fievet, J. P. Lagier, B. Blin, B. Beaudoin, and M. Figlarz, Solid State Ionics 32–33, 198 (1989).
[8]F. Dumitrache, I. Morjan, R. Alexandrescu, V. Ciupina, G. Prodan, I. Voicu, C. Fleaca, L. Albu, M. Savoiu, I. Sandu, E. Popovici, and I. Soare, Appl. Surf. Sci. **247**, 25 (2005).
[9]S. Calvin, E. E. Carpenter, and V. G. Harris, Phys. Rev. B **68**, 033411 (2003).
[10]L. R. Jordan, A. J. Betts, K. L. Dahm, P. A. Dearnley, and G. A. Wright, Corros. Sci. **47**, 1085 (2005).
[11]A. A. Hermas, M. Nakayama, and K. Ogura, Electrochim. Acta **50**, 2001 (2005).
[12]E. E. Carpenter, J. Magn. Magn. Mater. **225**, 17 (2001).